Volume 11
Number 5
May 2026
Pages 1165–1444

Nanoscale Horizons

The home for rapid reports of exceptional significance in nanoscience and nanotechnology

rsc.li/nanoscale-horizons

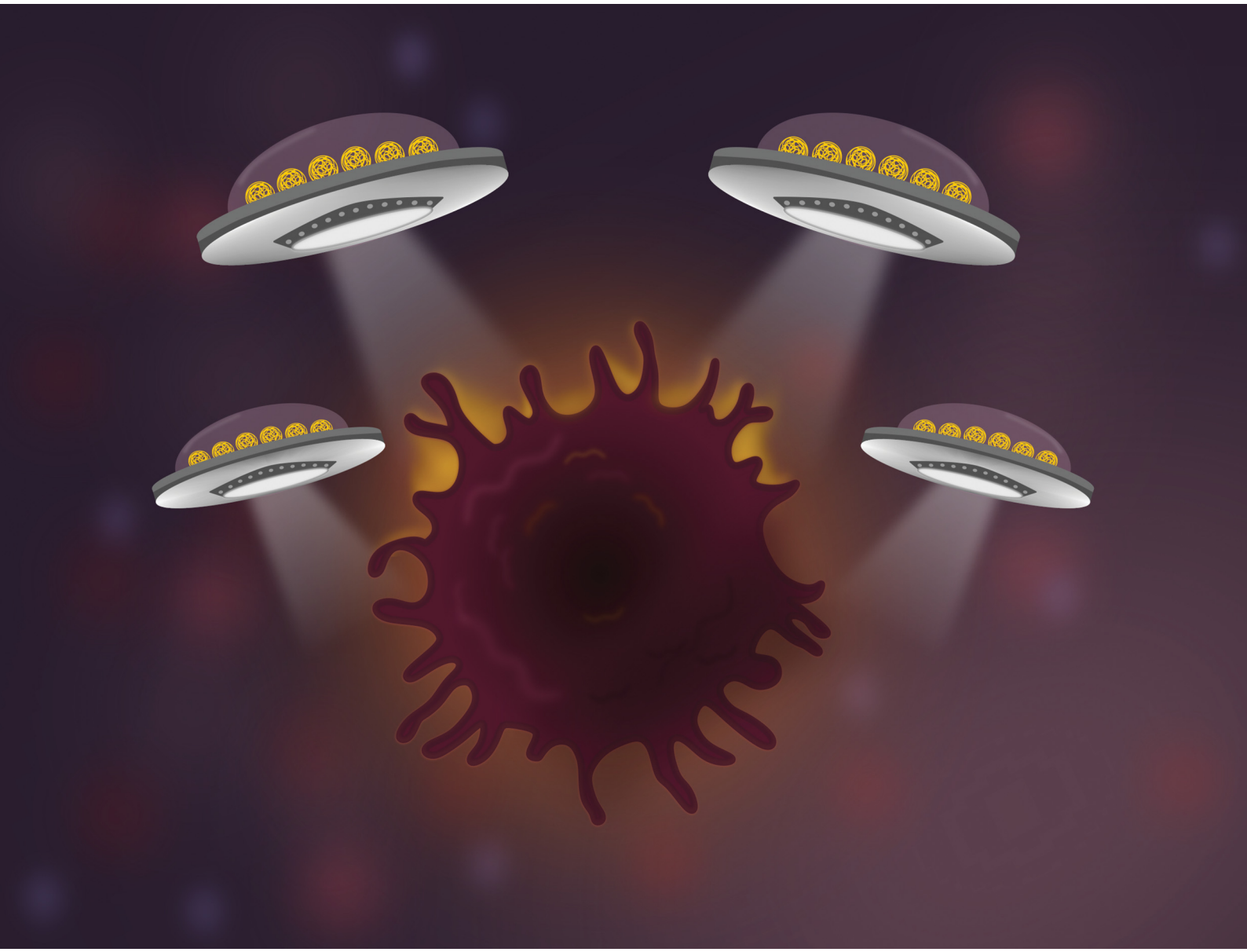

ISSN 2055-6756

ROYAL SOCIETY OF CHEMISTRY

COMMUNICATION

Jesús Martínez de la Fuente *et al.*
Controlled release of glucocorticoid *via* PLGA nanoparticles for modulating macrophage polarization in inflammation situations

NCNST

Nanoscale Horizons

ROYAL SOCIETY OF CHEMISTRY

COMMUNICATION

View Article Online
View Journal | View Issue

Cite this: *Nanoscale Horiz.*, 2026, **11**, 1302

Received 1st December 2025,
Accepted 6th March 2026

DOI: 10.1039/d5nh00782h

rsc.li/nanoscale-horizons

Controlled release of glucocorticoid *via* PLGA nanoparticles for modulating macrophage polarization in inflammation situations

Natalia Esteban-Pérez, [ab] Susel Del Sol-Fernández, [ac] Rafael Martín-Rapún [ab] and Jesús Martínez de la Fuente *[ab]

Glucocorticoids are among the most widely used anti-inflammatory and immunosuppressive drugs. However, their prolonged administration is associated with a wide range of adverse side effects including long-lasting immunosuppression. In this study, we aimed to encapsulate two commonly used glucocorticoids with different potency and duration, hydrocortisone and dexamethasone, into poly(lactic-*co*-glycolic acid) (PLGA) nanoparticles with the goal to modulate inflammatory gene expression in a delivery-dependent manner. We evaluated their anti-inflammatory properties in two *in vitro* models varying the timing of treatment administration based on lipopolysaccharide M1-polarized macrophages, key effectors of the innate immune system. Our results demonstrated that, for both strategies, drug-loaded nanoparticles significantly reduced the expression of interleukin-6, a pro-inflammatory cytokine, compared to the free drugs. However, in one of the strategies, while free drugs induced upregulation of interleukin-10, a key anti-inflammatory cytokine, no such effect was observed with the nanoparticle-based formulations. Overall, these results demonstrate that PLGA nanoparticles enable sustained glucocorticoid delivery and modulate inflammatory gene expression in activated macrophages in a delivery- and timing-dependent manner, providing comparative insight into how glucocorticoid delivery *via* PLGA nanoparticles shapes inflammatory gene regulation depending on treatment timing and highlighting the importance of *in vitro* model design.

New concepts

In our study, we present a conceptual advance in the administration of glucocorticoids by demonstrating that PLGA nanoparticles can decouple anti-inflammatory efficacy from unwanted immunosuppression. While conventional glucocorticoid therapy often triggers a compensatory upregulation of anti-inflammatory cytokines (such as IL-10), leading to excessive immunosuppression, our nanoparticle platform effectively reduces pro-inflammatory markers (IL-6) without triggering this immunosuppressive spike. Importantly, we show that therapeutic success relies heavily on the specific timing of administration during the inflammatory cycle. This highlights the need for chronotherapeutic approaches in nanomedicine. Consequently, our findings support a strategy for the selective modulation of macrophage polarization, offering a safer approach for treating chronic inflammation that moves beyond simple release kinetics.

Introduction

Glucocorticoids (GCs) are a class of steroid hormones widely used for their anti-inflammatory and immunosuppressive properties. They can be synthesised in the body under physiological conditions, as in the case of hydrocortisone (HC), or be synthetically modified to enhance potency and duration of action, such as dexamethasone (DEX).[1,2] These drugs are commonly prescribed to treat a broad range of conditions, including allergic reactions and chronic inflammatory diseases such as asthma,[3] rheumatoid arthritis,[4] and certain types of cancer.[5–7]

Over the years, several studies have explored the mechanisms by which GCs regulate the immune system. GCs are key modulators of the inflammatory response, exerting effects at multiple stages. During the initial, or "alarm" phase, they attenuate pro-inflammatory signalling pathways and suppress the production of inflammatory mediators, including nuclear factor kappa B (NF-κB) and various pro-inflammatory cytokines such as interleukin-1β (IL-1β), interleukin-6 (IL-6), and interferon- γ (IFN-γ). In the resolution phase, GCs promote the production of anti-inflammatory mediators, thereby facilitating the clearance of apoptotic cells and tissue debris through enhanced phagocytosis.[8,9] Importantly, GC effects vary significantly across different immune cell types, highlighting the complexity of their mechanism of action.[10,11]

[a] *Instituto de Nanociencia y Materiales de Aragón, INMA (CSIC-Universidad de Zaragoza), C/Pedro Cerbuna 12, 50009, Zaragoza, Spain. E-mail: j.m.fuente(at)csic.es*
[b] *Centro de Investigación Biomédica en Red de Bioingeniería, Biomateriales y Nanomedicina (CIBER-BBN), Madrid 28029, Spain*
[c] *Instituto de Ciencias Físicas, Universidad Nacional Autónoma de México, Av. Universidad s/n, Col. Chamilpa, Cuernavaca, Morelos 62210, Mexico*

However, the clinical use of GC presents a major challenge as they are mainly used for chronic pathologies and in contrast, side effects including hypertension, cataracts, immunosuppression, hyperglycaemia, osteoporosis, obesity and impaired wound healing show up mainly due to long-term therapies.[9,12] A promising strategy to mitigate GC-related adverse effects is the use of nanocarriers to enable a sustained release and thus, a more effective treatment. This approach would reduce the frequency of administration and maintain therapeutic drug levels for longer periods, potentially minimizing systemic exposure toxicity.[13] As a means to evaluate our hypothesis, in this study, we employed poly(lactic-*co*-glycolic acid) (PLGA) nanoparticles (NPs) encapsulating either HC or DEX. These two GCs differ significantly in their anti-inflammatory potency and pharmacokinetics, with DEX being approximately 26 times more potent than HC and exhibiting a longer duration of action.[14]

PLGA is a well-characterized, biocompatible, biodegradable polymer, approved by the U.S Food and Drug Administration (FDA) and the European Medicines Agency (EMA), and degrades into lactic and glycolic acid, which are naturally metabolized *via* the Krebs cycle. Previous studies have explored the encapsulation of DEX in PLGA NPs to enhance bioavailability and reduce toxicity;[15–17] however, comparative analyses between HC and DEX in the context of macrophage-mediated inflammation remain limited. Ultimately, this approach may contribute to the development of safer, more effective anti-inflammatory therapies for chronic conditions requiring long-term GC use.[18]

We employed macrophages as *in vitro* model to assess the immunomodulatory effects of GC-loaded NPs in comparison with the free drugs. Macrophages are key effectors of innate immunity and play a crucial role in initiating, sustaining, and resolving inflammation. They can originate either from circulating monocytes that migrate into tissues during inflammation, or from tissue-resident macrophages, which are an independent, self-renewing population derived from embryonic hematopoietic progenitors.[19–21]

Macrophages are highly plastic and can undergo polarization in response to environmental stimuli such as pro-inflammatory cytokines, bacterial products and signals derived from damaged or stressed tissues. This polarization results in two distinct functional phenotypes: classically activated macrophages (M1), which exhibit pro-inflammatory properties, and alternatively activated macrophages (M2), which are involved in anti-inflammatory responses, tissue repair and angiogenesis.[22]

M1 polarization is typically induced by lipopolysaccharide (LPS) and IFN- γ, leading to the secretion of inflammatory cytokines such as TNF-α, IL-1, and IL-6, and the expression of inducible nitric oxide synthase (iNOS). In contrast, M2 macrophages secrete anti-inflammatory cytokines such as interleukin-10 (IL-10), transforming growth factor β (TGF-β), and express surface markers as CD206 (mannose receptor). A key metabolic difference between these phenotypes lies in arginine metabolism: M1 macrophages use the iNOS pathway to produce citrulline and nitric oxide (NO), whereas M2 macrophages utilize the arginase pathway to generate ornithine and urea.[23] However, the dysregulation of macrophage polarization can lead to different chronic diseases such as rheumatoid arthritis.[24] Consequently, strategies aimed at repolarizing macrophages towards restorative phenotype have gained increasing attention.[25–27]

The aim of this study was to evaluate the immunomodulatory effects of HC and DEX when delivered *via* PLGA NPs, in comparison with their free forms, using an *in vitro* M1 macrophage model. While GC delivery *via* PLGA- based nanoformulations has been explored previously, most studies have focused on a single GC, and direct comparisons between GC of differing potency and pharmacokinetics under identical NP and *in vitro* conditions remain limited. By examining HC and DEX in parallel, this work investigates formulation-dependent factors, such as release kinetics, influence macrophage inflammatory responses beyond intrinsic drug potency.

Based on these considerations, we developed two experimental strategies using induced M1-polarized macrophages to better understand GC immunomodulation and to evaluate whether their effects are modified when delivered in NPs. In the first strategy, inflammatory stimulation and treatment were administered simultaneously (co-treatment approach), whereas in the second, macrophages were first stimulated with LPS to induce a predominant pro-inflammatory phenotype, followed by treatment with the GC formulations (pre-stimulation approach). This design enabled us to determine whether the therapeutic efficacy of GCs is influenced by the timing of administration relative to the inflammatory response.

Importantly, this study also highlights the relevance of an *in vitro* model design, demonstrating that identical nanoformulations can elicit distinct cellular responses depending on the experimental context in which they are evaluated.

Results and discussion

Synthesis and characterization of PLGA NPs loaded HC or DEX

PLGA NPs containing either HC or DEX were synthesized using the emulsion evaporation method (Fig. 1A).[28] To determine the optimal drug-to-PLGA ratio (μmol mg^{-1}) for each compound, a series of nanoformulations were prepared with varying ratios. The goal was to maximize drug loading (DL) while maintaining favorable physicochemical properties of the nanosystems.

As shown in Fig. 1B, both drugs exhibited an increasing trend in DL as the drug-to-PLGA ratio increased. However, this trend was disrupted at ratio of 3.5 suggesting a saturation point at which NPs could no longer incorporate additional drug. In the light of the results, a ratio of 2.5 was selected for further studies for, both HC and DEX, as it was the one that achieved the highest DL. At this ratio, HC-loaded NPs achieved a DL of 21.4% $\pm$ 1.4, while DEX-loaded NPs reached a DL of 25.1% $\pm$ 3.7. Encapsulation efficiency (EE) was 22.6% $\pm$ 0.8 in the case of HC-loaded NPs, while for DEX-loaded was 31.0% $\pm$ 3.1.

To evaluate colloidal stability, zeta-potential of NPs was measured in water. HC-loaded NPs showed a zeta potential of

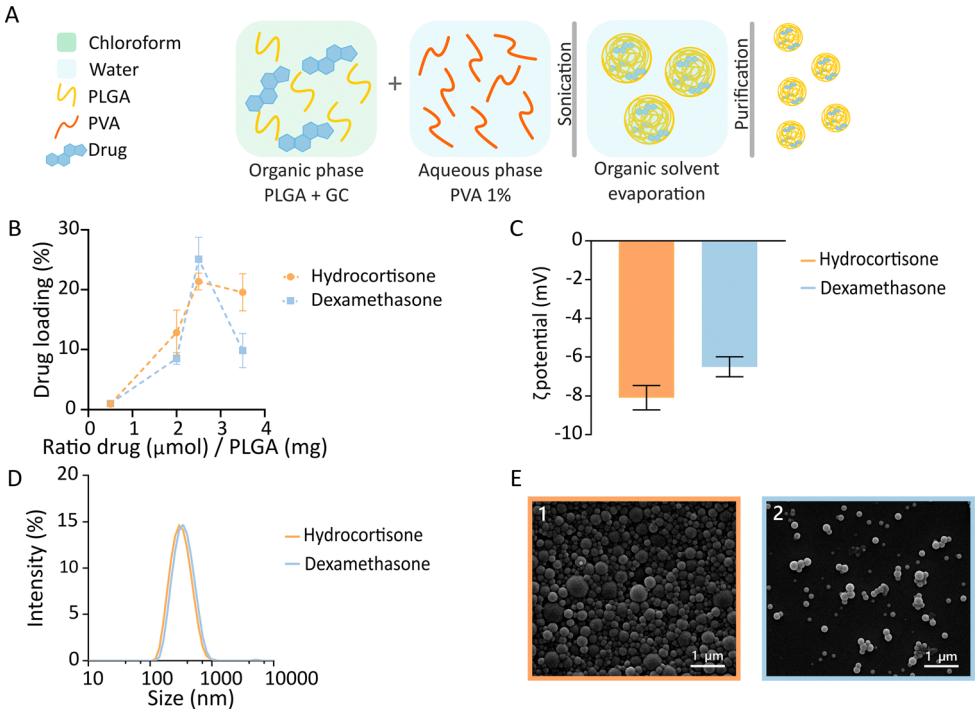

Fig. 1 Synthesis and physicochemical characterization of HC- and DEX-loaded PLGA NPs. (A) Schematic representation of emulsion-evaporation method for GCs loaded PLGA NPs synthesis. (B) Effect of drug-to- PLGA ratio on DL. Data is shown as mean ± standard deviation from three independent experiments. (C) ζ -potential measurements indicating the surface charge of both nanoformulations. (D) DLS analysis showing the average hydrodynamic diameter of HC- and DEX-loaded NPs. (E) SEM images of (E1) HC-loaded NPs and (E2) DEX-loaded NPs.

−8.1 ± 0.6 mV, whereas DEX-loaded ones of −6.5 ± 0.5 mV (Fig. 1C).

Nanoparticle size is a key parameter that can significantly influence *in vitro* uptake and is also crucial in determining the most appropriate route of administration.[29,30] In this study, NPs size was assessed by dynamic light scattering (DLS). HC-loaded NPs exhibited an average hydrodynamic diameter of 248 ± 20 nm while DEX-loaded NPs measured 275 ± 21 nm (Fig. 1D). In addition, the polydispersity index (PDI) of the HC-loaded NPs was 0.17 while the one of the DEX-loaded was 0.14, meaning in both cases monodisperse distributions. The size and charge difference between the two formulations was not significant, indicating that any differences in the *in vitro* behavior should be attributed to the drug rather than the physicochemical properties of the nanoformulations.

Additionally, NP morphology was characterized by scanning electron microscopy (SEM). In both HC- and DEX-loaded systems, NPs exhibited a uniform and spherical shape (Fig. 1E).

In vitro release studies

The release from PLGA NPs is affected by several parameters including polymer molecular weight, monomer composition, porosity and the interaction between the encapsulated payload and the polymer.[31] PLGA degradation and drug diffusion are the main mechanisms of drug release. One of the most characteristic PLGA-based NPs release profile is an initial burst release which is influenced by multiple factors including particle size, particle porosity, polymer weight, drug nature or aqueous boundary layer.[32,33] This is characterized by the rapid diffusion of the drug into the surrounding medium, which can lead to elevated concentrations of the free drug, potentially causing adverse effects. Moreover, it compromises the ability of the formulation to provide sustained release at the target site.

To evaluate the release profile of both nanoformulations, NPs were suspended in dialysis tubes and incubated in PBS at 37 °C under continuous agitation. Under these conditions, neither DEX-loaded NPs nor HC-loaded NPs exhibited a significant burst release, confirming efficient drug encapsulation. However, the two formulations displayed distinct release profiles. After 6 h, approximately 25% of the DEX was released into the medium, whereas only about 10% of HC was released under the same conditions. At 24 h, HC-loaded NPs reached 25% cumulative release, while DEX-loaded NPs had released around 60% of the encapsulated drug (Fig. 2). Thus, the release rate of DEX-loaded NPs was approximately 2.3-fold faster than that of HC-loaded NPs. The DEX release profile observed in this study was also observed by Saraf *et al.*[34] and Costello *et al.*[35]

Despite these differences in initial release kinetics, both formulations exhibited sustained release over 48 hours. By this time point, DEX-loaded NPs reached approximately 80% cumulative release, whereas HC-loaded NPs released around 50% of the encapsulated drug. Both drugs exhibited a biphasic release profile, characterized by an initial release phase up to 24 h that transitioned into a plateau, followed by a second phase of sustained release. This biphasic behaviour was observed for both formulations, although it was more pronounced for DEX.

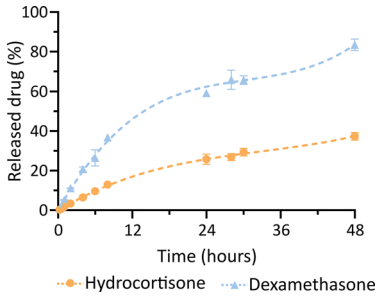

Fig. 2 Release profile of HC- and DEX-loaded PLGA NPs over time. Data indicates the percentage of drug released from each formulation over the tested period. The results are expressed as the mean ± SD from three independent experiments.

Due to its greater hydrophobicity, DEX is likely less tightly entrapped within the PLGA matrix, resulting in a faster and more accentuated release. Overall, the biphasic release observed for both drugs highlight the potential of PLGA NPs as effective nanocarriers capable of sustaining drug release for at least 48 h, thereby minimizing the need for repeated administrations within this period of time.

In vitro studies. Cytocompatibility and NP uptake

One of the main advantages of nanoformulations is their ability to control drug release and act as effective carriers, potentially reducing systemic toxicity and adverse effects.[36,37] Therefore, in this study, we aimed to determine whether there were differences in cytotoxicity between the encapsulated and non-encapsulated forms of the drugs in macrophages cells. PLGA is a widely used polymer for micro- and nanoformulations due to its biocompatibility and biodegradability.[38] To assess the cytocompatibility of the HC- and DEX-loaded NPs, MTT assays were performed with different concentrations ranging from 0.1 mg mL^{-1} to 0.3 mg mL^{-1}. In parallel, equivalent free-drug concentrations were calculated based on NP DL, representing the theoretical maximum drug content within the NPs (20 to 60 μg mL^{-1} for free HC and 15 to 45 μg mL^{-1} for free DEX). This approach acknowledges that free drugs are immediately bioavailable, whereas encapsulated drugs require release from the carrier prior to cellular action.

Since both NPs did not achieve a complete drug release until 48 hours but drug metabolism can occur during this time, MTT assays were conducted after 48 hours of treatment exposure. As expected, both HC- and DEX-loaded NPs were non-cytotoxic across the tested concentrations (Fig. 3A and B). In contrast, free HC showed a dose-dependent reduction in cell viability, while free DEX did not induce any cytotoxic effects. This difference can be attributed to the sustained release profile of NPs, as in the case of HC-loaded ones, only about 50% of the encapsulated drug would be available to the cells after 48 h.

To confirm PLGA NP uptake by macrophages, fluorescently labelled NPs were prepared using Nile Red. These NP exhibited size and surface charge similar to the GC-loaded formulations. Internalization studies showed that after 24 h approximately

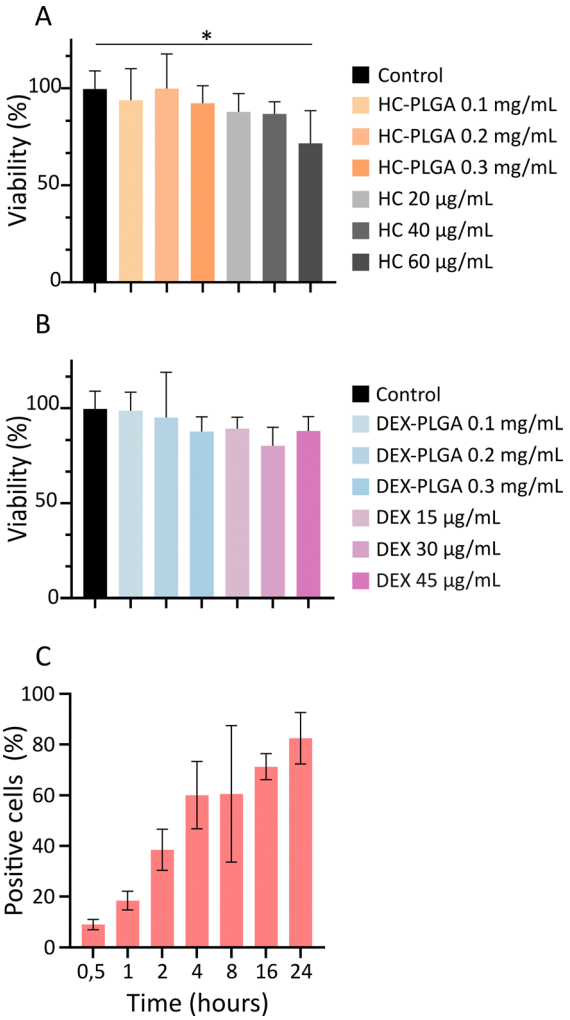

Fig. 3 Cytocompatibility and cellular uptake of HC- and DEX-loaded PLGA nanoparticles in RAW 264.7 macrophages. (A) Effect of HC-loaded NPs and free HC and (B) DEX-loaded NPs and free DEX treatments on cell viability after 48 h, assessed by MTT assay. Cell viability was expressed as a percentage relative to untreated control cells. Statistical significance was determined using one-way ANOVA followed by Tukey's multiple comparison test ($p < 0.05$). Three biological replicates were conducted. (C) Uptake of Nile Red-loaded PLGA NPs by RAW 264.7 during 24 h.

80% of the cell population was fluorescent (Fig. 3C), indicating efficient nanoparticle incorporation.

Immunomodulatory effects of HC and DEX loaded PLGA NPs using M1-polarized macrophage *in vitro* model

To evaluate the immunomodulatory effects of GC-loaded NPs in M1-polarized macrophages we developed two treatment strategies: (1) Concomitant treatment: RAW 264.7 macrophages were simultaneously exposed to LPS and either free or GC -loaded NPs for 48 hours and (2) Treatment after LPS stimulation: macrophages were first stimulated with LPS for 24 hours to induce predominant M1 phenotype, followed by treatment with free or GC-loaded NPs for 48 hours (Fig. 4A and B).

To polarize macrophages to M1, RAW 264.7 cell line was exposed to different concentrations of LPS (1 μg mL^{-1}

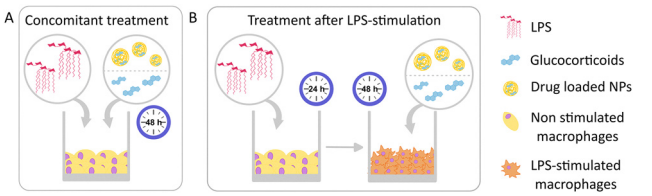

Fig. 4 Schematic representation of the two treatment strategies used to evaluate the immunomodulatory effects of glucocorticoid-loaded nanoparticles in M1-polarized macrophages. (A) Concomitant treatment: RAW 264.7 macrophages were simultaneously exposed to LPS and either free or NP-encapsulated GC for 48 hours. (B) Treatment after LPS stimulation: macrophages were first stimulated with LPS for 24 hours to induce M1 phenotype, followed by treatment with free or NP-encapsulated GC for 48 hours.

and 5 μg mL^{-1}). After 6 h of stimulation, LPS-exposed cells exhibited noticeable morphological changes, appearing larger and with more protrusions in comparison with control cells (Fig. S1A in the SI).[39] However, no morphological differences could be observed between the two LPS concentrations tested. After 24 hours, more pronounced alterations were observed: cells displayed numerous vacuoles in the cytoplasm and appeared more elongated (Fig. S1A in the SI).

The Griess reagent was used to measure nitrite levels in cell media as indirect indicator of NO cell production. In this colorimetric assay, nitrites react with sulfanilamide to form a diazonium salt, which subsequently reacts with *N*-1-naphtylethylenediamine dihydrochloride (NED), resulting in the formation of a coloured dye (Fig. S1B in the SI). Although morphological changes were already evident 6 h after LPS exposure, NO production could not be detected using Griess assay until 48 h post-stimulation. Moreover, no significant differences in nitrite levels were found between the two LPS concentrations tested (1 μg mL^{-1} and 5 μg mL^{-1}), suggesting a plateau in the cellular response within this range (Fig. S1C in the SI). Based on these findings, a concentration of 1 μg mL^{-1} LPS was selected for subsequent experiments as no differences between them were seen and overstimulation was not desired as it could cause cell death.

Additionally, immunofluorescence assays were performed to assess the expression of CD38 as marker of M1 and CD206 as marker of M225. CD38 showed a markedly increased expression in LPS-stimulated cells compared to control cells indicating successful M1 polarization. However, basal expression in control cells was observed (Fig. S2A in the SI). In contrast, CD206 expression did not show significant differences between control and LPS-stimulated cells (Fig. S2B in the SI), which is expected as M2 polarization did not take place.

GC loaded-NP efficacy in reducing NO production

To assess potential dose-dependent effects, NPs concentrations ranging from 0.1 to 0.3 mg mL^{-1} were tested. In parallel, equivalent amounts of free drug were administered based on NPs DL to allow a comparative evaluation between the NP-encapsulated and free forms under identical experimental conditions.

For concomitant treatment, after 48 h exposure with LPS and NPs or the free drug, Griess assay revealed that both HC- and DEX-loaded NPs reduced NO production (Fig. 5A and B). In the case of HC-loaded NPs, the highest concentration resulted in a 35% reduction in NO production compared to LPS-stimulated positive control. Notably, DEX-loaded NPs due to its higher anti-inflammatory potency produced a more pronounced effect, leading to a reduction of nearly 50% in NO production. When considering the free drugs, a clear

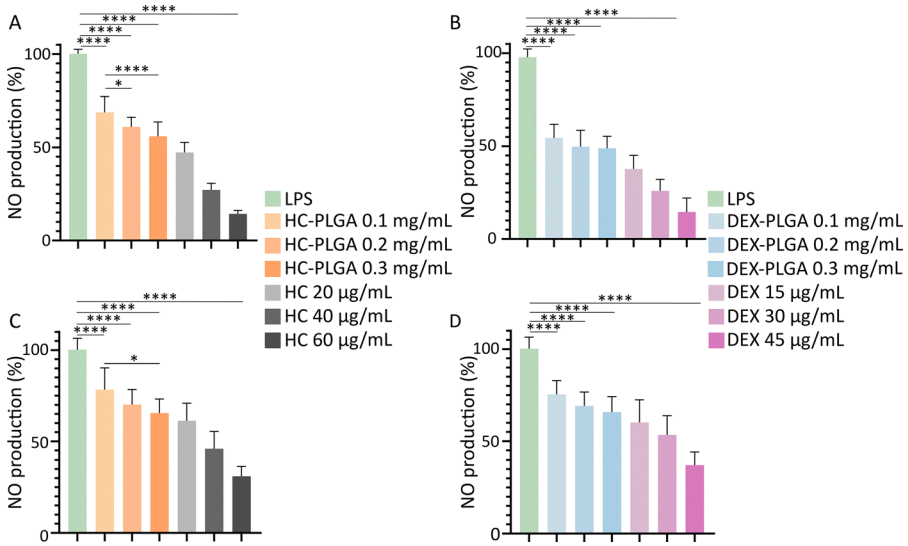

Fig. 5 NO cell production assessed by Gries assay for: the concomitant treatment with LPS and either (A) HC-loaded NPs and free HC; or (B) DEX-loaded NPs and free DEX; the treatment after 24 h-LPS cell exposition with either (C) HC-loaded NPs and free HC; or (D) DEX-loaded NPs and free DEX. Data are presented as mean ± standard deviation. Statistical analysis was performed using one-way ANOVA followed by Tukey's multiple comparison test (*$p < 0.05$, ****$p < 0.0001$). $n = 3$.

dose-dependent reduction in NO levels was observed for both HC and DEX, with DEX showing a stronger inhibitory effect across all concentrations tested. However, it is important to consider that NP release is not fully accomplished within 48 h, which may influence the observed response and must be taken into account when interpreting the results.

In the case of LPS pre-stimulation strategy, cells were pre-stimulated over 24 h with LPS, after which the medium was replaced with fresh medium containing the treatment over 48 h. Under these conditions, both HC- and DEX-loaded NPs were still able to reduce NO concentration (Fig. 5C and D). However, no marked differences were observed when compared to the concomitant treatment. Interestingly, free HC and DEX were less effective in these conditions than during co-treatment. Although they still induced a reduction in NO production compared to untreated cells, their anti-inflammatory effect was slightly lower than the observed in concomitant strategy, suggesting that the timing of drug administration influences the development of the inflammatory response.

Although free drugs appeared to induce a greater reduction in NO production within the experimental window, it is important to highlight that Griess assay quantifies the cumulative amount of NO produced throughout the entire assay. In the case of NP treatment, sustained release may delay the drug availability and lead to an underestimation of the NP-associated response when using this method, as the assay reflects total NO accumulation from the beginning of the treatment to the endpoint.

While free drugs are immediately bioavailable, NP-mediated delivery provides prolonged exposure to the active compound, which may lead to a slower onset of detectable NO production in the experimental frame.

Effects of GC-loaded NPs on Pro- and anti-inflammatory gene expression

To gain a more precise understanding the inflammatory regulation of GC-loaded NPs compared with free drugs, mRNA levels of key inflammation-related genes were quantified using RT-qPCR. For subsequent analyses, the highest concentrations of both the nanoformulations and the free drug were selected, as these conditions produced the most pronounced biological effects in previous assays. Three genes were selected: iNOS, IL-6 and IL-10. iNOS was included as a classical marker of M1 macrophage activation and to further corroborate results obtained by Griess Assay (Fig. 5). IL-6 and IL-10 were assessed as representative pro-inflammatory and anti-inflammatory cytokines, respectively.

Under concomitant treatment, iNOS expression was significantly reduced across all four treatment groups compared to LPS-stimulated control (Fig. 6A), with no significant differences were observed between formulations. These results indicate that both free and NP-encapsulated GCs effectively downregulated iNOS expression under the tested conditions. Given the sustained-release profile of the nanoformulations, transcriptional readouts

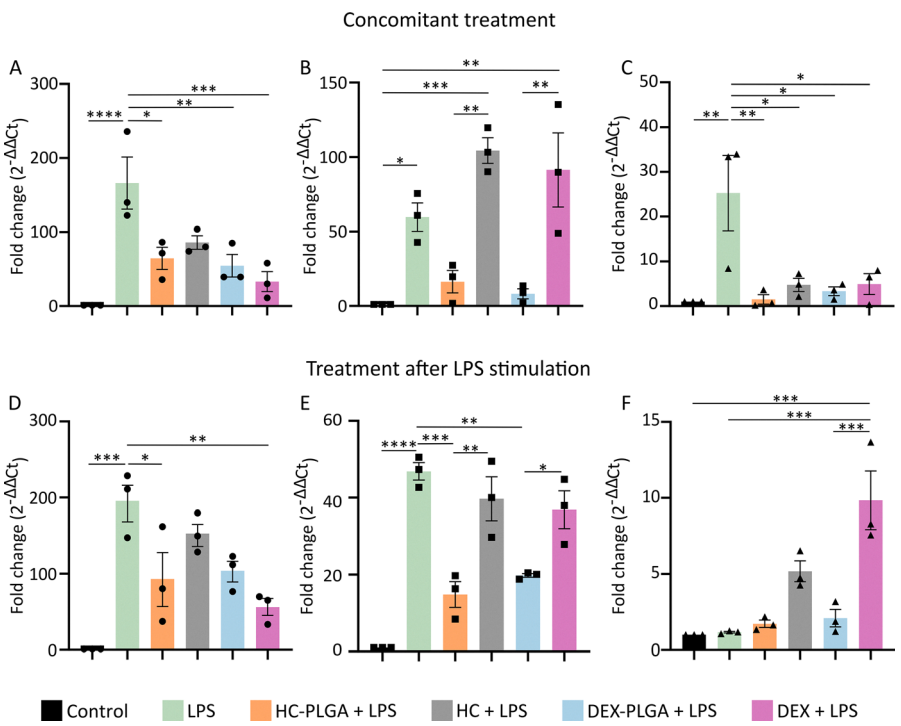

Fig. 6 RT-qPCR analysis of iNOS, IL-6 and IL-10 expression in RAW 264.7. Results expressed as fold change ($2^{-\Delta\Delta Ct}$) relative to untreated control. Concomitant treatment results for (A) iNOS, (B) IL-6 and (C) IL-10. Treatment after 24 h- LPS cell exposition results for (D) iNOS, (E) IL-6 and (F) IL-10. Data shown as mean ± SEM. Statistical analysis was performed using one-way ANOVA followed by Tukey's multiple comparison test (*$p < 0.05$, **$p < 0.01$, ***$p < 0.001$ ****$p < 0.0001$). $n = 3$.

may capture regulatory effects that are not fully reflected by cumulative NO measurements.

In contrast, IL-6 was markedly overexpressed in both the LPS control group and cells treated with free drugs, whereas reduced expression was detected in cells treated with the NP formulations (Fig. 6B). Similar results were observed by Sun *et al.*[40] suggesting that the delivery platform of GC can influence IL-6 regulation under inflammatory conditions. While free GCs partially modulate inflammation activation, immediate availability may not be sufficient to prevent LPS-driven IL-6 overexpression under the experimental condition tested. In comparison, NP-treated cells exhibited a distinct IL-6 expression profile, which may be related to differences in drug exposure kinetics associated with controlled release.

IL-10 was overexpressed in LPS-stimulated control cells, which may indicate a compensatory mechanism intended to modulate the inflammatory response and promoting cell survival.[41] No significant overexpression was observed in any of the treated groups, with no significant differences among them (Fig. 6C). Although GC are commonly associated with M2c[42] responses, the absence of IL-10 upregulation suggests that transcriptional regulation may differ depending on the delivery system. This effect could be related to differences in drug exposure time or to the altered availability of the drug resulting from encapsulation.

In the pre-stimulation strategy, iNOS showed similar pattern as observed in concomitant treatment. Initial 24 h LPS exposure induced iNOS overexpression, which was reduced in all treatment groups with no significant differences between formulations (Fig. 6D), indicating comparable capacity to downregulate iNOS expression regardless of drug delivery method.

IL-6 expression after LPS pre-stimulation showed similar profile as in concomitant strategy, overexpression occurred in both the LPS stimulated and free-drug-treated cells, but not in those treated with NPs. This consistent pattern suggests that controlled release influences IL-6 transcriptional regulation in activated macrophages under the conditions examined (Fig. 6E).

IL-6 is a key pro-inflammatory cytokine involved not only in the acute-phase immune response, but also in the progression to chronic inflammation and autoimmune diseases including rheumatoid arthritis, inflammatory bowel disease, and cytokine release syndromes.[43–45] Therefore, its downregulation through sustained GC delivery by NPs may be relevant for understanding how controlled release systems influence inflammatory signalling pathways *in vitro*. Compared with free drugs, which are immediately bioavailable, NP formulations provide a prolonged exposure to GCs, which may contribute to differential transcriptional dynamics. This observation supports the potential of NP-based systems in managing conditions where long-term modulation of IL-6 is desirable.

IL-10 expression exhibited distinct behaviour under the pre-stimulation strategy. LPS induced cells without treatment did not show IL-10 overexpression. Interestingly, elevated IL-10 levels were observed in cells treated with the free drugs that was not observed in the concomitant strategy, while no overexpression occurred in those treated with NPs formulations (Fig. 6F). These findings indicate that sustained drug release *via* PLGA NPs influences *in vitro* inflammatory gene expression, particularly in previously activated macrophages.

Experimental

Materials

PLGA (lactide: glycolide (75 : 25), mol wt 66 000–107 000), PVA (average M_w 146 000–186 000, 87–89% hydrolyzed), HC, DEX, methanol (MeOH) and chloroform were purchased from Sigma-Aldrich. Mini Dialysis kit 8 kDa cut-off, 250 μL was purchased from GE Healthcare Bio-Sciences Corp. Piscotawa, NJ 0885-1327, USA. RAW 264.7 cell line (ATCC number TIB-71) was purchased from ATCC. Phosphated buffer saline (PBS, 1X, pH 7.4, Gibco), Dulbecco's modified Eagle Medium (DMEM, Gibco) were purchased from Thermo Fischer. Fetal bovine serum (FBS), glutaMAX, Griess reagent kit assay (ref. MAK367) and LPS from *Salmonella enterica* serotype typhimurium was purchased from Sigma-Aldrich. CD38 (ref. PA5-89326) and CD206 (ref. PA5-101657) polyclonal antibodies, AlexaFluor™ 488 goat anti-rabbit (ref. A11008) and AlexaFluor™ 555 goat anti-rabbit (ref. A32732) from Invitrogen were purchased from Thermo Fischer. Isolation Kit and RT-qPCR master mix were purchased from NZYtech. Primers were obtained from Biomers (Table S1).

Methods

Nanoparticle synthesis. Nanoparticles were synthesized by emulsion evaporation method. Poly(vinyl alcohol) (PVA) was chosen as surfactant. Organic phase consisting of 50 mg of PLGA and the drug or Nile Red, was dissolved in 2.5 mL of chloroform : MeOH (7 : 1). Subsequently, 5 mL of 1% PVA was added (aqueous phase). The emulsion was formed by sonication at 40% amplitude for 5 min (UP400 St Ultrasonic Homogenizer, Hielscher Ultrasonics, Teltow, Germany).

Afterwards, the suspension was left overnight to allow the organic solvent to evaporate. Nanoparticles were purified through a two-step centrifugation process: initial centrifugation at 4.000 g for 2 min where the pellet was discarded for removing the biggest nanoparticles and a second centrifugation at 20.000 g for 20 min. The supernatant was discarded to take away the unencapsulated drug, and the resulting pellet was resuspended in 3 mL of deionized water. To enhance long-term stability, nanoparticles were lyophilized with 0.5% mannitol as a cryoprotectant.

Nanoparticle characterization. Dynamic light scattering (DLS) analysis and surface potential (Zeta potential) measurements were carried out using a Malvern Zetasizer Nano ZS (Malvern Panalytical Ltd., Malvern, United Kingdom). Nanoparticle hydrodynamic diameter, polydispersity index (PDI) and Zeta potential were measured in water at concentration of 0.1 mg mL^{-1} at 25 °C using polystyrene latex refraction index. Scanning Electron Microscopy (SEM) sample observation was carried out using F-50 Inspect (FEI Company, Thermo Fisher Scientific) at 10 kV.

Encapsulation efficiency and drug loading. Encapsulation efficiency (EE) was defined as mg of drug in the final suspension per mg of drug added to the synthesis and drug loading (DL) was defined as mg of drug per mg of NPs.

For the calculation of EE and DL, 0.25 mg of nanoparticles were disrupted by dissolving them in 500 μL of methanol and sonicated for 30 minutes. After sonication, the suspension was filtered with a filter 0.22 μm pore size and analyzed by High Performance Liquid Chromatography (HPLC). HPLC measurements were performed on a Shimadzu Prominence-i LC-2030C 3D HPLC system with a PDA detector and a Phenomenex Luna Omega 5 μm C18 100 Å LC column (150 mm × 4.6 mm). As eluents water and acetonitrile were used. The chromatographic gradient consisted in 35% of acetonitrile for 8 min, followed by 2 min linear increase to 95% maintained during 6 minutes. The acetonitrile concentration was then decreased to 35% in 4 min. Linear calibration curves passing through the origin were obtained for both compounds. The regression equation for hydrocortisone was y (μg mL^{-1}) = 3.99 × 10^{-5}x (R^2 = 0.999), and for dexamethasone y (μg mL^{-1}) = 6.06 × 10^{-5}x (R^2 = 0.999) (Fig. S3 in the SI).

***In vitro* release studies.** Release studies were conducted in PBS (pH 7.4) using dialysis tubes at 37 °C under constant agitation. To perform the experiment, 2 mg of nanoparticles were placed inside a dialysis tube and placed in a glass vial containing 4 mL of PBS assessing sink conditions.

At predetermined time intervals (0.25, 0.5, 1, 2, 4, 6, 24, 28, 30 and 48 hours), 300 μL of the release medium were taken out and replaced with an equal volume of fresh PBS. The collected samples were filtered and analyzed by HPLC to quantify the amount of drug released over time.

Cell culture. Murine macrophage cell line (RAW 264.7) was cultured in Dulbecco's modified Eagle's medium (DMEM) supplemented with 10% FBS, 5% L-glutamine, and 5% penicillin/streptomycin antibiotics and maintained in a humidifier incubator at 37 °C in a 5% CO_2 atmosphere.

Cell viability assay. MTT assay was performed to evaluate cell viability of NPs treated cells. RAW 264.7 cells (2 × 10^4 cells/well) were seeded in a 96-well plate for 24 h. After, medium was replaced and cells were treated with different concentrations of HC- or DEX-loaded PLGA NPs (0.1 to 0.3 mg mL^{-1}) or the corresponding amount of free drug for 48 h at 37 °C. Cells were thoroughly washed with PBS, and 10 μl of MTT solution (5 mg mL^{-1} in PBS) in a final volume of 100 μL cDMEM was added to each well. Following 30 min of incubation at 37 °C, the plates were centrifugated at 2500 rpm for 15 minutes and formazan salts were dissolved with 100 μl of DMSO in agitation for 15 min at 37 °C; the resulting absorbance was determined at λ = 570 nm on a microplate reader (Thermo Scientific Multiskan GO MA, USA).

Cellular uptake. RAW 264.7 cells (2 × 10^4 cells/well) were seeded in 100 μL of cDMEM in a 96-well plate for 24 h. The medium was then replaced with 0.1 mg mL^{-1} Nile Red-loaded NPs in cDMEM. At the designated time points, medium was removed, and cells were washed twice with PBS. Cells were detached with 50 μL of Accutase and incubated at 37 °C for 5 min. Subsequently, 150 μL of cDMEM were added, and cells were collected and centrifuged for 15 s at 10 000 g. The supernatant was discarded, and cells were resuspended in 400 μL of PBS. Fluorescence was measured using CytoFLEX flow cytometer (Beckman Coulter Life Sciences, Indianapolis, IN, USA) with a 488 nm laser and Nile Red fluorescence was detected in the ECD-A channel. Data were analyzed using CytExpert 2.4 software (Beckman Coulter).

Nitrite quantification by griess assay. RAW 264.7 cells (2 × 10^4 cells/well) were seeded in 100 μL of cDMEM in a 96-well plate for 24 h. After, for the concomitant treatment the medium was replaced by cDMEM containing 1 μg mL^{-1} LPS and the treatment (GC-loaded NPs or free drug). After 48 hours of treatment, Griess Assay was performed according to manufacturer instructions for Nitrite Assay Kit (Griess Reagent): 10 μL of Griess reagent I, 10 μL of Griess reagent II and 80 μL of cell medium were mixed in a well plate and read after 10 min at 540 nm. In the case of the treatment after LPS stimulation, cDMEM containing 1 μg mL^{-1} LPS was applied to the cells for 24 h, after the medium was replaced by fresh medium containing the treatments for 48 h when the Nitrite Assay kit was performed in the same conditions as described previously.

Immunofluorescence. Raw 264.7 cells (2 × 10^4 cells/well) were seeded onto 14 nm glass coverslips placed in a 24-well plate for 24 h. Cells were stimulated with 1 μg mL^{-1} of LPS for 48 h. After, cells were washed three times with PBS and fixed with 2% PFA for 10 min at RT. After fixation, cells were blocked with 2% BSA in PBS for 1 h at RT to prevent nonspecific binding. Primary antibody (CD38, ref. PA5-89326 or CD206, ref. PA5-101657) incubation was performed for 1 h at RT in blocking buffer, followed by two washes with PBS. Cells were then incubated with secondary antibody AlexaFluor™ 488 goat anti-rabbit (ref. A11008) or AlexaFluor™ 555 goat anti-rabbit (ref. A32732) for 1 h at RT in 1% BSA. After that, cells were washed with PBS twice. Nuclei were stained with DAPI for 10 min at RT. Finally, coverslips were mounted onto glass slides using FluorSave mounting medium. Fluorescence microscopy images were performed using an inverted microscope (Nikon Eclipse Ti-E, Amsterdam, The Netherlands) equipped with a sCMOS camera (Sona 4B, Andor).

RT-qPCR. Cells were treated as previously mentioned in the nitrite quantification assay. After the treatment was completed, cells were washed with PBS and detached of the plate. Cells were centrifugated 1200 rpm for 5 min to obtain a pellet. Total RNA was extracted using the Total RNA Isolation Kit (NZYtech) according manufacturer's instructions. First-strand cDNA was synthesized with High-Capacity cDNA Reverse Transcription Kit (Applied Biosystem), also following the supplier's instructions. RT-qPCR was carried out using NZY master mix (NZYtech) in a CFX Opus 96 Real-Time PCR System (Bio-Rad). For RT-qPCR amplification, the following cycling steps were used: initial 2 min at 50 °C, 5 min at 95 °C, followed by 40 cycles at 95 °C for 15 s, 60 °C for 1 min. In addition, melting curves (from 60 to 95 °C, increment 0.5 °C) were generated to check any undesired amplification products. GADPH was used as a reference gene and relative expression

levels were calculated using the delta–delta Ct ($2^{-\Delta\Delta CT}$) method (Table S1 in the SI).

Statistical analysis

Data is expressed as mean ± SD of three biological replicates in all cases. The RT-qPCR results are shown as mean ± SEM. Statistical analysis was performed using GraphPad Prism 8.0.2.

Conclusions

In this study, HC- and DEX-loaded PLGA NPs were successfully developed and characterized. Both formulations exhibited an average size of approximately 250 nm and showed sustained release over 48 h. In addition, 2.5 drug-PLGA ratio was selected to achieve efficient DL reaching approximately 20% for both GC. *In vitro* cytocompatibility assays confirmed that both nanoparticle formulations were well tolerated by RAW 264.7 macrophages under the tested conditions.

RAW 264.7 macrophages were successfully polarized into M1 and used as *in vitro* model to evaluate the immunomodulatory effects of GC-loaded NPs. The two treatment strategies -concomitant administration and treatment after LPS stimulation- showed different cellular responses highlighting the influence of treatment timing. In both approaches, GC-loaded NPs and free drugs were able to significantly reduce NO production, with differences consistent with the known relative potency of GC. RT-qPCR analyses showed a comparable downregulation of iNOS expression for both NPs and the free drugs.

Analysis of inflammatory cytokine gene expression revealed that GC-loaded NPs were more effective preventing IL-6 overexpression than free drugs in both treatment strategies. In contrast, IL-10 overexpression was observed only in the treatment after LPS stimulation only in the case of free GC, suggesting that drug delivery mode and release kinetics may influence transcriptional inflammatory regulation.

Overall, these results indicate that PLGA NPs enable sustained delivery of GC, allowing modulation of inflammatory gene expression in activated macrophages in a manner that differs from free GC administration. This study provides comparative insight into how GC potency, release kinetics, and timing of administration shape macrophage inflammatory responses *in vitro*. Importantly, these findings highlight the relevance of experimental design and treatment timing when evaluating nanoformulations as identical delivery systems may elicit distinct cellular responses depending on the inflammatory context.

Author contributions

N.E.P.: conceptualization, investigation, data curation, methodology, formal analysis and writing-original draft. S.DS.F.: conceptualization, data curation, writing-review & editing. R.M.R: conceptualization, supervision, writing – review & editing. J.M.F.: conceptualization, supervision, funding acquisition, resources, writing-review & editing.

Conflicts of interest

There are no conflicts to declare.

Data availability

Additional raw data are available from the corresponding author upon reasonable request.

The data supporting the findings of this study are available within the article and its Supplementary Information (SI). The supplementary information provides additional data on LPS-induced macrophage morphological changes and nitrite production, immunofluorescence staining of polarization markers CD38 and CD206, HPLC calibration curves for hydrocortisone and dexamethasone, and primer sequences used for RT-qPCR analysis. See DOI: https://doi.org/10.1039/d5nh00782h.

Acknowledgements

This work has been supported by the grants CEX2023-001286-S, PID2020-118485RB-I00 and PID2022-141276OB-I00 funded by MCIN/AEI/10.13039/501100011033 and ERDF (EU). The research has also been funded by CIBER-Consorcio Centro de Investigación Biomédica en Red-(CB16/01/00263) from Instituto de Salud Carlos III (Spanish Ministry of Science and Innovation and European Commission, European Regional Development Fund). N.E.P. acknowledges financial support from Gobierno de Aragón Predoctoral Fellowship program (2022). S. D. S.-F. acknowledges Marie Skłodowska-Curie Postdoctoral Fellowships (HORIZON-MSCA-2021-PF-01-01, Grant agreement No. 101064735) funded by the European Union. The authors are also grateful to Gobierno de Aragón and ''ERDF A way of making Europe'' for funding the Bionanosurf (E15_20R) research group.

Notes and references

1 S. L. Swartz and R. G. Dluhy, *Drugs*, 1978, **16**, 238–255.
2 G. J. Martinez, M. Appleton, Z. A. Kipp, A. S. Loria, B. Min and T. D. Hinds, *Physiol. Rev.*, 2024, **104**, 473–532.
3 E. Heffler, L. N. G. Madeira, M. Ferrando, F. Puggioni, F. Racca, L. Malvezzi, G. Passalacqua and G. W. Canonica, *J. Allergy Clin. Immunol.:Pract.*, 2018, **6**, 776–781.
4 C. Hua, F. Buttgereit and B. Combe, *RMD Open*, 2020, **6**, 536.
5 L. T. Warris, M. M. Van Den Heuvel-Eibrink, F. K. Aarsen, S. M. F. Pluijm, M. B. Bierings, C. Den Van Bos, C. M. Zwaan, H. H. Thygesen, W. J. E. Tissing, M. A. Veening, R. Pieters and E. L. T. Van Den Akker, *J. Clin. Oncol.*, 2016, **34**, 2287–2293.
6 R. S. Goodman, D. B. Johnson and J. M. Balko, *Clin. Cancer Res.*, 2023, **29**, 2580–2587.
7 A. Faggiano, R. Mazzilli, A. Natalicchio, V. Adinolfi, A. Argentiero, R. Danesi, S. D'Oronzo, S. Fogli, M. Gallo, D. Giuffrida, S. Gori, M. Montagnani, A. Ragni, V. Renzelli, A. Russo, N. Silvestris, T. Franchina, E. Tuveri, S. Cinieri,

A. Colao, F. Giorgino and M. C. Zatelli, *Crit. Rev. Oncol. Hematol.*, 2022, **180**, 103826.
8 D. W. Cain and J. A. Cidlowski, *Nat. Rev. Immunol.*, 2017, **17**(4), 233–247.
9 U. Baschant and J. Tuckermann, *J. Steroid Biochem. Mol. Biol.*, 2010, **120**, 69–75.
10 L. M. Franco, M. Gadkari, K. N. Howe, J. Sun, L. Kardava, P. Kumar, S. Kumari, Z. Hu, I. D. C. Fraser, S. Moir, J. S. Tsang and R. N. Germain, *J. Exp. Med.*, 2019, **216**, 384–406.
11 V. S. Madamsetty, R. Mohammadinejad, I. Uzieliene, N. Nabavi, A. Dehshahri, J. García-Couce, S. Tavakol, S. Moghassemi, A. Dadashzadeh, P. Makvandi, A. Pardakhty, A. A. Afshar and A. Seyfoddin, *ACS Biomater. Sci. Eng.*, 2022, **8**, 1763–1790.
12 U. Baschant and J. Tuckermann, *J. Steroid Biochem. Mol. Biol.*, 2010, **120**, 69–75.
13 M. A. Tryfonidou, G. de Vries, W. E. Hennink and L. B. Creemers, *Adv. Drug Delivery Rev.*, 2020, **160**, 170–185.
14 J. Lockett, W. J. Inder and V. L. Clifton, *Endocr. Rev.*, 2024, **45**, 593–624.
15 B. Boltnarova, A. Durinova, L. Jandova, S. Micuda, O. Kucera, I. Pavkova, M. Machacek, I. Nemeckova, M. Vojta, J. Dusek, M. Krutakova, P. Nachtigal, P. Pavek and O. Holas, *Macromol. Biosci.*, 2024, **25**, 2400411.
16 A. Arranz-Romera, B. M. Davis, I. Bravo-Osuna, S. Esteban-Pérez, I. T. Molina-Martínez, E. Shamsher, N. Ravindran, L. Guo, M. F. Cordeiro and R. Herrero-Vanrell, *J. Controlled Release*, 2019, **297**, 26–38.
17 S. Rençber, F. Aydın Köse and S. Y. Karavana, *Pharm. Dev. Technol.*, 2020, **25**, 149–158.
18 F. Danhier, E. Ansorena, J. M. Silva, R. Coco, A. Le Breton and V. Préat, *J. Controlled Release*, 2012, **161**, 505–522.
19 Z. Wang, A. L. Koenig, K. J. Lavine and R. S. Apte, *Trends Immunol.*, 2019, **40**, 825–841.
20 A. Shapouri-Moghaddam, S. Mohammadian, H. Vazini, M. Taghadosi, S. A. Esmaeili, F. Mardani, B. Seifi, A. Mohammadi, J. T. Afshari and A. Sahebkar, *J. Cell. Physiol.*, 2018, **233**, 6425–6440.
21 M. D. Park, A. Silvin, F. Ginhoux and M. Merad, *Cell*, 2022, **185**, 4259–4279.
22 P. Rodríguez-Morales and R. A. Franklin, *Trends Immunol.*, 2023, **44**, 986–998.
23 K. R. Peterson, M. A. Cottam, A. J. Kennedy and A. H. Hasty, *Trends Pharmacol. Sci.*, 2018, **39**, 536–546.
24 C. Yunna, H. Mengru, W. Lei and C. Weidong, *Eur. J. Pharmacol.*, 2020, **877**, 173090.
25 J. Hwang, M. Zheng, C. Wiraja, M. Cui, L. Yang and C. Xu, *Nanoscale Adv.*, 2020, **2**, 5254–5262.
26 H. Gao, R. Cheng, I. Cardoso, M. Lobita, I. Pacheco-Fernández, R. Bártolo, L. R. Rodrigues, J. Hirvonen and H. A. Santos, *Nano Lett.*, 2025, **25**, 2831–2840.
27 H. Wei, H. Huang, H. He, Y. Xiao, L. Chun, Z. Jin, H. Li, L. Zheng, J. Zhao and Z. Qin, *Research*, 2024, **7**, 0540.
28 K. Y. Hernández-Giottonini, R. J. Rodríguez-Córdova, C. A. Gutiérrez-Valenzuela, O. Peñuñuri-Miranda, P. Zavala-Rivera, P. Guerrero-Germán and A. Lucero-Acuña, *RSC Adv.*, 2020, **10**, 4218–4231.
29 J. Dolai, K. Mandal and N. R. Jana, *ACS Appl. Nano Mater.*, 2021, **4**, 6471–6496.
30 M. J. Mitchell, M. M. Billingsley, R. M. Haley, M. E. Wechsler, N. A. Peppas and R. Langer, *Nat. Rev. Drug Discovery*, 2020, **20**, 101–124.
31 D. J. Hines and D. L. Kaplan, *Crit. Rev. Ther. Drug Carrier Syst.*, 2013, **30**, 257–276.
32 J. Yoo and Y. Y. Won, *ACS Biomater. Sci. Eng.*, 2020, **6**, 6053–6062.
33 K. Öztürk, M. Kaplan and S. Çalış, *Int. J. Pharm.*, 2024, **666**, 124799.
34 I. Saraf, V. Kushwah, C. Alva, I. Koutsamanis, J. Rattenberger, H. Schroettner, C. Mayrhofer, D. Modhave, M. Braun, B. Werner, K. Zangger and A. Paudel, *Mol. Pharm.*, 2023, **20**, 1307–1322.
35 M. A. Costello, J. Liu, L. Kuehster, Y. Wang, B. Qin, X. Xu, Q. Li, W. C. Smith, N. A. Lynd and F. Zhang, *Mol. Pharm.*, 2023, **20**, 6330–6344.
36 Z. Chenxi, A. Hemmat, N. H. Thi and M. Afrand, *J. Mol. Liq.*, 2025, **424**, 126999.
37 M. J. Mitchell, M. M. Billingsley, R. M. Haley, M. E. Wechsler, N. A. Peppas and R. Langer, *Nat. Rev. Drug Discovery*, 2020, **20**, 101–124.
38 M. Mir, N. Ahmed and A. Ur Rehman, *Colloids Surf., B*, 2017, **159**, 217–231.
39 F. Heinrich, A. Lehmbecker, B. B. Raddatz, K. Kegler, A. Tipold, V. M. Stein, A. Kalkuhl, U. Deschl, W. Baumgärtner, R. Ulrich and I. Spitzbarth, *PLoS One*, 2017, **12**, e0183572.
40 R. Sun, X. Liu, Y. Zhang, Q. Li, Y. Zhu and C. Fan, *Particuology*, 2023, **73**, 1–7.
41 S. T. Yeung, L. J. Ovando, A. J. Russo, V. A. Rathinam and K. M. Khanna, *Cell Rep.*, 2023, **42**, 112171.
42 G. Zizzo, B. A. Hilliard, M. Monestier and P. L. Cohen, *J. Immunol.*, 2012, **189**, 3508.
43 F. Pandolfi, L. Franza, V. Carusi, S. Altamura, G. Andriollo and E. Nucera, *Int. J. Mol. Sci.*, 2020, **21**, 5238.
44 S. Kang, T. Tanaka, M. Narazaki and T. Kishimoto, *Immunity*, 2019, **50**, 1007–1023.
45 T. Tanaka, M. Narazaki, K. Masuda and T. Kishimoto, *Adv. Exp. Med. Biol.*, 2016, **941**, 79–88.